IJASST International Journal of Applied Sciences and Smart Technologies

Volume 07
Issue 01

p-ISSN 2655-8564, e-ISSN 2685-943, pp. 83-98, 2025

Bubble Flow Configurations Generated by Ejector Type Bubble Generator

IGNB. Catrawedarma [1*], Sefri Ton [2], Dadang Dwi Pranowo [3], Fredy Surahmanto [4], Achilleus Hermawan Astyanto [5,6]

[1]*Department of Mechanical Engineering, Politeknik Negeri Banyuwangi, Jalan Raya Jember Km. 13, Kabat, Banyuwangi 68461, Indonesia*
[2]*Department of Agribusiness, Politeknik Negeri Banyuwangi, Jalan Raya Jember Km. 13, Kabat, Banyuwangi 68461, Indonesia*
[3]*Department of Civil Engineering, Politeknik Negeri Banyuwangi, Jalan Raya Jember Km. 13, Kabat, Banyuwangi 68461, Indonesia*
[4]*Department of Mechanical Engineering Education, Universitas Negeri Yogyakarta, Yogyakarta 55281, Indonesia*
[5]*Department of Mechanical Engineering, Universitas Sanata Dharma, Kampus III USD Maguwoharjo, Yogyakarta 55282, Indonesia*
[6]*Center for Smart Technology Studies, Universitas Sanata Dharma, Kampus III USD Maguwoharjo, Yogyakarta 55282, Indonesia*
[*]*Corresponding Author: ignb.catrawedarma@poliwangi.ac.id*

(Received 18-12-2024; Revised 05-01-2025; Accepted 06-01-2025)

Abstract

Bubble flow configurations generated by an ejector bubble generator were captured using a high-speed video camera and extracted into several images. The air flow and nozzle diameter were varied during the test in ranges of 0.1-1.5 lpm and 1.17-3.5 mm, respectively. The results reveal that in general the bubble flow structure coming out from the bubble generator is divided into three regions, namely the entrance, bubble swarm, and bubble dispersed region. It is found that there is a higher time delay of bubble production when the air flow and the nozzle diameter decrease. On the other hand, the bubble production time is longer, if the air flow and the nozzle diameter increase.

Keywords: Bubble swarm and dispersed regions, bubble delayed dan generated times

1 Introduction

Microbubble generators are a new and emerging technology with extensively potential applications in numerous industries, such as medicine, where they are utilized

This work is licensed under a Creative Commons Attribution 4.0 International License

as a contrast agent in ultrasound examinations to improve the appearance of tissues or organs [1], [2]. In addition, airlift pump systems use microbubbles to lift water and sediment [3]–[6], while wastewater treatment employs them to diminish oil, heavy metals, and tiny particulates in water via the flotation processes [7], [8]. Here, microbubbles possess a high surface area, enabling them to expedite molecular interactions in the chemical industry [9]. Therefore, microbubbles are frequently employed to cleanse fresh products, disinfect food items, and sanitize equipment within the food sectors [10], [11]. On the other hand, microbubbles in the shipping sector also minimize drag on the ship's outer surface, thereby reducing fuel consumption [12].

However, several problems associated with microbubbles' utilization encompass sustaining stability across diverse conditions and attaining a reliable cost-effective manufacturing scale for specific applications. Consequently, various researchers persistently engage in research and development to enhance the utilization of microbubbles and address current issues. They have innovated bubble formation methods, such as reducing the channel cross-section to increase the flow velocity, which in turn increases the shear force and breaks the bubble into a smaller diameter. Included in this method are orifice [13]–[15], venturi [16]–[24], and spherical body [25] types of microbubble generators. Another innovation employs swirl flow to harness centrifugal force for enhancing shear force [26]–[29].

The orifice type features a design characterized by an abrupt decrease in cross-section to enhance fluid velocity, which concurrently elevates the loss of flow energy. Meanwhile, the design of the spherical body, minimizing the cross-section at the channel's periphery instead of its center, poses issues in both production and maintenance. On the other hand, the swirl flow configuration leads to considerable energy dissipations, requiring a pump with substantial capacity to transport water. Therefore, Basso et al. [30] and Terasaka et al. [31] designed a venturi type with a stepwise cross-sectional reduction to minimize flow energy losses, hence enhancing its economic efficiency. Moreover, the venturi type offers the benefits of simple installation and maintenance [32], and it generates bubbles with a smaller diameter while maintaining the same operational parameters as other types [33], [34]. In a mean time, the incorporation of air gap and porous pipes on the air inlet side was executed to achieve a reduced bubble size

distributions [14], [35]–[37]. Additionally, researchers have also used multistage venturi and swirl-venturi combinations to achieve a smaller bubble diameter [27], [28], [38].

Next, Huang et al. [32] synthesized the effects of diverse geometric and operational parameters on venturi-type microbubble generators. The results enhance that the bubble size is inversely proportional to the water discharge, but it is proportional to the air discharge as also implied on several reports [16], [17], [36], [39]. Here, the air discharge has a smaller effect on the size and distribution of bubbles than the water discharge because the bubble rupture is highly dependent on the flow turbulence. Another, augmenting the throat length and divergence angle or reducing the throat and outlet diameters in a venturi-type bubble generator results in a reduction of the bubble diameter [40]. Here, the convergence angle, diameter, and number of air holes have almost no effect on the bubble diameter as also reported by several others [19], [41]. Therefore, the throat diameter and divergence angle play an important role in the performance of the venturi bubble generator.

The present study employs an ejector bubble generator, a variant of the venturi bubble generator in which a similar ejector's working principle was briefly described on the report of Mardikus [42]. Here, the ejector bubble generator utilizes a tapered cross-section at the water input to reduce flow energy loss, and includes supplementary air space prior to the amalgamation of air and water to increase bubbles' production. Investigations toward the detailed characteristics of the bubble generator were carried out by varying the input air flow as a part of the operational parameters and the nozzle diameter as particular geometric parameters. The configuration of the bubble flow emerging from the bubble generator was examined utilizing a high-speed camera. Changes in the time delay and the duration of bubble formation were investigated to determine the optimum value of the pair of the air flow and nozzle diameter.

2 Material and Methods

In the present investigation, a procedure on the experiment, conducted at the Mechanical Engineering Workshop of Politeknik Negeri Banyuwangi, commencing with the assembly of an ejector bubble generator, is schematically illustrated in Fig. 1(A). The water input diameter of the bubble generator, D, was 7 mm, while the nozzle diameter, d,

was adjusted from 1.17 to 3.50 mm. The ejector bubble generator was positioned 5 cm above the base of the test pool, exactly at the midpoint of its width. The test pool was 100 cm in length, 50 cm in width, and 50 cm in height; it was constructed from transparent glass and filled with water to a depth of 45 cm, as depicted in Fig. 1(B).

The data collection was initiated by activating a 12 VDC water pump to supply water to the bubble generator. The water discharge was constantly set at 5.0 liters per minute (lpm) using a water flowmeter. The air discharge flowing from the aerator was regulated from 0.1 to 1.5 lpm through an air flowmeter for each nozzle diameter. Subsequently, the amalgamation of water and air in the ejector bubble generator produced bubbles that were expelled and integrated with the water in the test pool. The bubble flow was captured with a Sony ZV-1 high-speed camera at 1000 frames per second (fps), with a shutter speed of 1/12800, an aperture of f8.0, and an ISO of 4000. The distance from the lens to the central output of the ejector bubble generator was 30 cm. A series of 50 W LED lamps was mounted behind the test pool to enhance the illumination, with a diffused

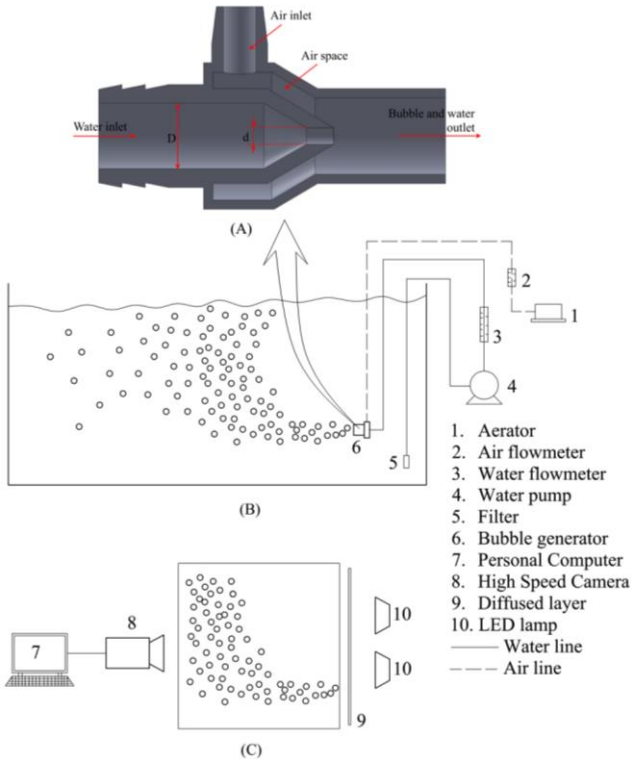


Figure 1. (A) Detail of ejector MBG, (B) Apparatus schematic, (C) Image capturing schematic

layer to achieve a uniform lighting, as depicted in Fig. 1(C). The video of the bubble flow emitted from the bubble generator for each air discharge and nozzle diameter was subsequently recovered into multiple images using MATLAB software to analyze the flow structures, time delays, and created durations.

3 Results and Discussions

3.1. Bubble flow configurations

Fig. 2 illustrates the standard flow configurations when the bubble exits the bubble generator's outlet. Here, flow areas can be grouped into entrance, bubble swarm, and bubble dispersed regions. The entrance region is the closest area to the bubble generator outlet, and the influence of the turbulent flow (yellow line) is very strong on this particular area. This area is referred to a ligament as reported by Mawarni et al.[43] or a mixing shock by Cramers et al.[44]. Next, the flow regions that occur in the ejector include a configuration of jet flow, mixing shock and bubble flow. The jet flow area exhibits a low pressure which drastically increases when it enters the mixing shock area and tends to be stable in the bubble flow area. The mixing shock area has a high rate of energy dissipation, turbulence, and shear stress. It produces small bubbles and increases the interfacial area. Visually, it can be seen that if the air flow increases from Qg = 0.1 lpm to Qg = 1.5 lpm, there is an increase in the entrance length. When the bubble comes out of the outlet, there is another increase in the flow acceleration due to the changes in the momentum between the bubble and the water in the pool.

On the other hand, due to the influence of the hydrostatic force of the water, there is a deceleration in the flow of the previously produced bubble. It causes a high turbulent bubble flow to penetrate the bubble flow that has previously come out. Collisions, ruptures, and amalgamations of bubbles transpire during this penetration. Both, collisions between the bubbles, and also collisions between bubbles and water, respectively, cause an interface instability. Here, if a light fluid is configured below a heavier fluid in a gravitational field, the lighter fluid will press the heavier fluid so that the interface of the two fluids is unstable to small disturbances. However, Rayleigh–Taylor instability states that interface instability between two fluids occurs due to differences in the density. This

interface instability occurs when there is a constant acceleration that leads from the heavy fluid to the light fluid [45]. Additionally, Kelvin-Helmholtz instability also implies that the interface between two fluids becomes unstable if there is a jump in tangential velocity towards the interface. Here, the interface instability between two fluids is caused by differences in velocity [46].

Hence, in the bubble swarm region the influence of turbulent flow begins to decrease, and several bubbles start to separate for evenly distributed. The breaking and coalescing of bubbles begin to occur. The bubble fragments into smaller pieces as a result of the water's hydrodynamic force, which surpasses the bubble's surface tension. The hydrodynamic force of water is generated by the erratic motion of the water and the bubbles emanating from the bubble generator's output. The break of this bubble causes a smaller bubble diameter, which causes the surface tension to become more significant and the rising velocity to become lower. It flows to the red circle with the dotted line in the bubble dispersed area.

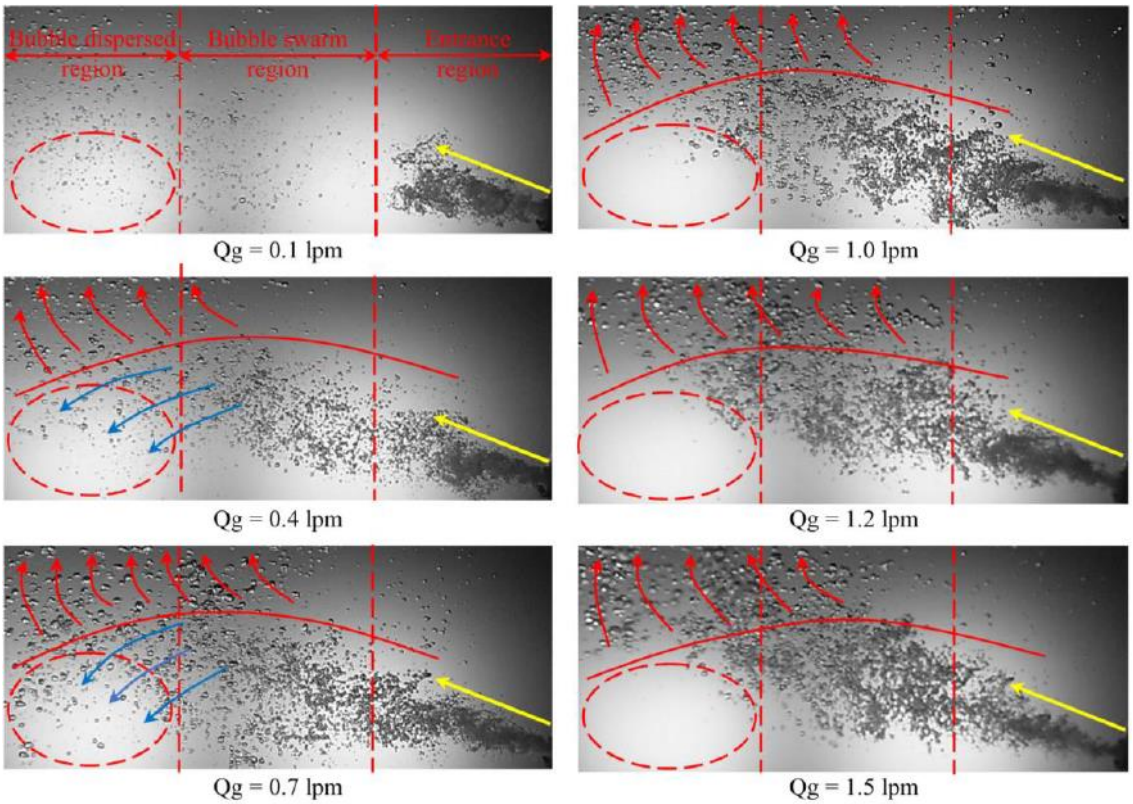


Figure 2. Flow structure in various air flow rate at d = 1.40 mm

Moreover, the bubble flows dispersed in the bubble dispersed region, characterized by the formation of larger bubbles flowing towards the top, as shown by the red arrow. In contrast, bubbles with smaller diameters flow towards the bottom, as indicated by the blue arrow. The circle with the dotted line shows the difference in the small bubble flow area in the bubble dispersed region. Here, the more air flow increases, the fewer bubbles are in the circle with the dotted line. It further shows that the greater the air flow, the larger the diameter of the bubble generated so that its volume is larger. This enhances a buoyancy and ascent velocity of the bubble while reducing its residence period, facilitating upward movement.

Fig. 2 shows that at the air flow Qg = 0.1 lpm, there is a stagnant bubble flow caused by a delay in bubble production time between the first bubble in the dispersed bubble region and the second bubble production in the entrance region. Different phenomena occur when the air discharge increases from Qg = 0.4 lpm to Qg = 1.5 lpm with a shorter bubble production delay time. The smaller water discharge causes this delayed time, and two-phase flow pressure at the outlet of bubble generator becomes lower due to a lower friction between the phases [47]. The low contact area between the phases causes the lower friction between phases due to the smaller bubbles formed when the air flow is lower. Thus, bubbles are smaller when the air flow is lower due to the lower inertial force. The bubble formation process is caused by ‘competition’ between inertial force and the bubble's surface tension. More bubbles are produced when the surface tension exceeds the inertial force.

3.2. Bubble-delay and Bubble-generation Times

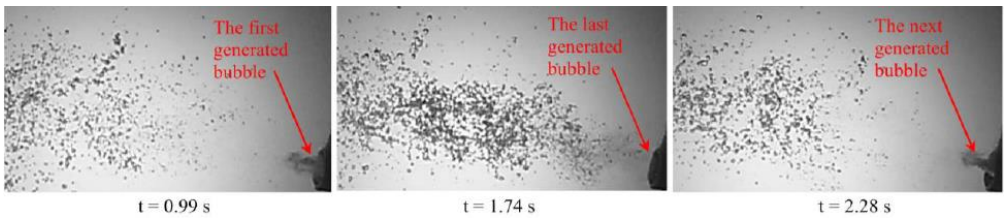
One of the factors that affects the performance of the microbubble generator in increasing dissolved oxygen is the number of generated microbubbles. Therefore, when the time delay is longer, the number of bubbles generated is less so that the concentration of dissolved oxygen is lower. Fig. 4 shows the effect of air flow and nozzle diameter on waiting time for bubbles to come out from the ejector and time to produce bubbles. The intermittent nature of the bubble emanating from the ejector output results in a delay in bubble formation.

Fig. 3(A) illustrates the procedure for quantifying bubble-delay and bubble-generation's durations. The video of the bubble formation was extracted in several images, and then the bubble-delay and bubble-generation times were identified. Bubble-generation time is the time needed to produce bubbles or the initial time the bubble comes out from the outlet until it stops coming out. Here in the picture, when t = 0.99 s, the bubble started to flow out of the bubble generator's outlet and moved away until it was separated from the outlet as at t = 1.74 s. A bubble-generation time is determined by subtracting the final time of bubble formation from the initial time, so that here in particular, the bubble-generation time equals to 1.74-0.99 = 0.74 s. After t = 1.74 s, the bubble does not come out of the ejector outlet, and the bubble starts to come out again at t = 2.28 s. The time from t = 1.74 s to t = 2.28 s is called bubble-delay time. Therefore, bubble-delay time is the time to wait until a new bubble produces from the ejector outlet. Here, bubble-delay time is determined by the time of a new generated bubble minus the time of the last generated bubble, so from Fig. 3(A), we get bubble-delay time equals to 2.28-1.74 = 0.54 s.

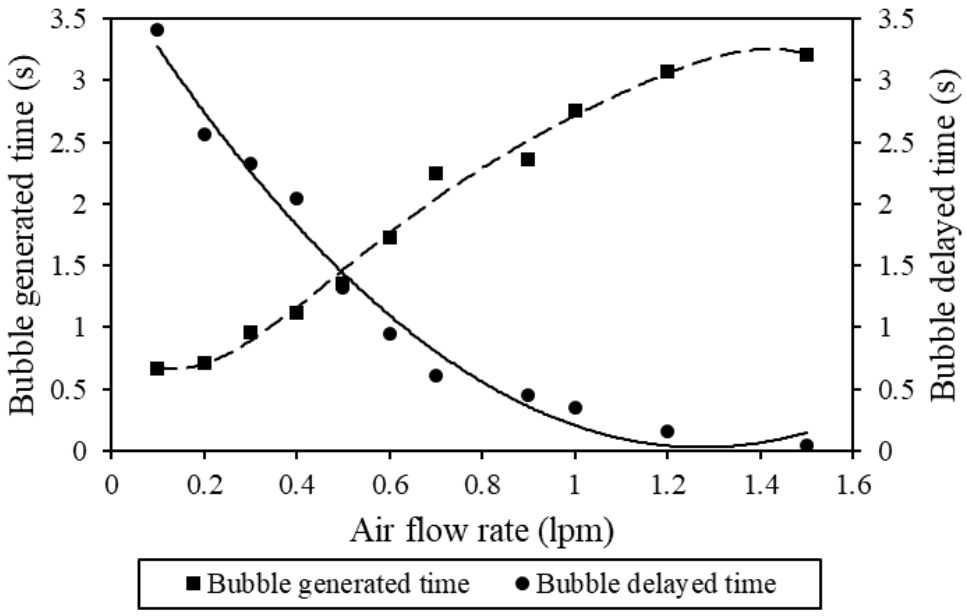
Fig. 3(B) presents the influence of air discharge on generated and delayed times. The solid line shows the trend line of bubble-delayed time, and the dotted line depicts the bubble-generated time. The greater the air flow at a constant nozzle diameter, the more significant the decrease in bubble-delayed time and the increase in bubble-generated time. It is caused by the influence of the higher flow velocity when the air discharge is more significant. The higher velocity causes the inertial force to be greater, so the two-phase flow pressure at the bubble generator outlet is more significant. It causes the two-phase flow's ability to penetrate the water in the pool to be greater, and the waiting time for the bubble production becomes shorter. It shows that when the air flow supplied to the bubble generator increases, the bubbles form more smoothly without delay. The intersection of the trendline of delayed and generated time occurs at an air discharge of 0.5 lpm, which means that the generated water discharge and the delayed time are almost the same.

Fig. 3(C) shows the effect of nozzle diameter on bubble generated and delayed times. When the nozzle diameter is larger, there is a decrease in the delayed time and an increase in the bubble generated time. It is strongly influenced by a physical phenomenon in which the larger the nozzle diameter, the greater the contact angle between the fluid

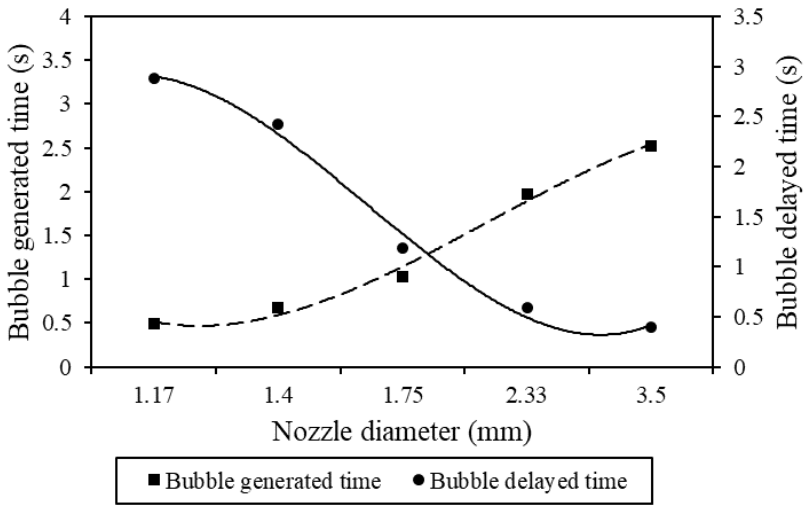
and the outlet wall. The greater the contact angle, the smaller the throat area and the shorter the low-pressure area. It allows more bubbles to be sucked in and implicates the longer the bubble generated time. The intersection point of the generated trendline and delayed time occurs at a nozzle diameter of 1.75 mm, with the shortest time difference. It reveals that the nozzle diameter of 1.75 mm is the optimum dimension since there is no significant difference between the bubble-generation and the bubble-delay times.



(A)



(B)



(C)

Figure 3. (A) Measurement of generated and delayed time, (B) Generated and delayed bubbles time for various air flow rate at d = 1.4 mm, (C) Generated and delayed bubbles time for various nozzle diameter at Qg = 0.1 lpm

4 Conclusions

The investigations on the bubble flow configurations generated by bubble generator-type ejectors were conducted to ascertain the bubble flow characteristics, the periods of bubble generation, and the delays in bubble formation for different air discharge rates and nozzle sizes. The results are as follows:

- The bubble flow from the ejector bubble generator is classified into the entrance, bubble swarm, and bubble-dispersed regions. The division of this area is based on the influence of the turbulent flow from the bubble generator outlet, which decreases as the bubble gets further away from the outlet.
- In the bubble formation process using an ejector bubble generator, it is revealed that the time delay in the bubble generated is shorter when the air flow rate is lower and the nozzle diameter is smaller. The duration of bubble generation increases with a higher airflow rate and a larger nozzle diameter. The condition with an air flow rate of 0.5 lpm and a nozzle diameter of 1.75 mm provides an optimum performance for bubble-delayed and bubble-generated times.

Acknowledgements

The authors would like to express a deepest gratitude to Indonesia Endowment Fund for Education Agency (Lembaga Pengelola Dana Pendidikan/LPDP) and Direktorat Pendanaan Riset dan Inovasi, National Research and Innovation Agency (Badan Riset dan Inovasi Nasional/BRIN) for the financial support through the Riset dan Inovasi untuk Indonesia Maju (RIIM-4) scheme with contract number 136/IV/KS/11/2023.

References

[1] S. S. Dastgheyb and J. R. Eisenbrey, Microbubble Applications in Biomedicine, in Handbook of Polymer Applications in Medicine and Medical Devices, Elsevier (2014) pp. 253–277, doi: 10.1016/B978-0-323-22805-3.00011-6.

[2] A. Sridharan, J. R. Eisenbrey, P. Machado, E. D. deMuinck, M. M. Doyley, and F. Forsberg, Delineation of Atherosclerotic Plaque Using Subharmonic Imaging Filtering Techniques and a Commercial Intravascular Ultrasound System, *Ultrason Imaging*, vol. 35, no. 1, pp. 30–44, Jan. 2013, doi: 10.1177/0161734612469511.

[3] IGNB. Catrawedarma, Deendarlianto, and Indarto, Statistical Characterization of Flow Structure of Air – water Two-phase Flow in Airlift Pump – Bubble Generator System, *International Journal of Multiphase Flow*, vol. 138, no. 103596, pp. 1–16, 2021, doi: 10.1016/j.ijmultiphaseflow.2021.103596.

[4] I. Catrawedarma, Deendarlianto, and Indarto, The performance of airlift pump for the solid particles lifting during the transportation of gas-liquid-solid three-phase flow : A comprehensive research review, *Proc IMechE Part E: J. Process Mechanical Engineering*, vol. 0, no. 0, pp. 1–23, 2020, doi: 10.1177/0954408920951728.

[5] G. Ligus, D. Zajac, M. Masiukiewicz, and S. Anweiler, A new method of selecting the airlift pump optimum efficiency at low submergence ratios with the use of image analysis, *Energies*, vol. 12, no. 4, 2019, doi: 10.3390/en12040735.

[6] P. Enany, O. Shevchenko, and C. Drebenstedt, Experimental Evaluation of Airlift Performance for Vertical Pumping of Water in Underground Mines, *Mine Water and the Environment*, vol. 40, no. 4, pp. 970–979, 2021, doi: 10.1007/s10230-021-00807-w.

[7] S. Khuntia, S. K. Majumder, and P. Ghosh, Microbubble-aided water and wastewater purification: a review, *Reviews in Chemical Engineering*, vol. 28, no. 4–6, Jan. 2012, doi: 10.1515/revce-2012-0007.

[8] C. Liu *et al.*, Effect of microbubble and its generation process on mixed liquor properties of activated sludge using Shirasu porous glass (SPG) membrane system, *Water Research*, vol. 46, no. 18, pp. 6051–6058, Nov. 2012, doi: 10.1016/j.watres.2012.08.032.

[9] R. Parmar and S. K. Majumder, Microbubble generation and microbubble-aided transport process intensification—A state-of-the-art report, *Chemical Engineering and Processing: Process Intensification*, vol. 64, pp. 79–97, Feb. 2013, doi: 10.1016/j.cep.2012.12.002.

[10] J. Lu, O. G. Jones, W. Yan, and C. M. Corvalan, Microbubbles in Food Technology, *Annu. Rev. Food Sci. Technol.*, vol. 14, no. 1, pp. 495–515, Mar. 2023, doi: 10.1146/annurev-food-052720-113207.

[11] H. Zhang and R. V. Tikekar, Air microbubble assisted washing of fresh produce: Effect on microbial detachment and inactivation, *Postharvest Biology and Technology*, vol. 181, p. 111687, Nov. 2021, doi: 10.1016/j.postharvbio.2021.111687.

[12] A. Hashim, O. B. Yaakob, K. K. Koh, N. Ismail, and Y. M. Ahmed, Review of micro-bubble ship resistance reduction methods and the mechanisms that affect the skin friction on drag reduction from 1999 to2015, *Jurnal Teknologi*, vol. 74, no. 5, pp. 105–114, 2015, doi: 10.11113/jt.v74.4650.

[13] N. Dietrich, N. Mayoufi, S. Poncin, N. Midoux, and H. Z. Li, Bubble formation at an orifice: A multiscale investigation, *Chemical Engineering Science*, vol. 92, pp. 118–125, Apr. 2013, doi: 10.1016/j.ces.2012.12.033.

[14] W. E. Juwana, A. Widyatama, O. Dinaryanto, W. Budhijanto, Indarto, and Deendarlianto, Hydrodynamic characteristics of the microbubble dissolution in liquid using orifice type microbubble generator, *Chemical Engineering Research and Design*, vol. 141, pp. 436–448, Jan. 2019, doi: 10.1016/j.cherd.2018.11.017.

[15] S. H. Marshall, M. W. Chudacek, and D. F. Bagster, A model for bubble formation from an orifice with liquid cross-flow, *Chemical Engineering Science*, vol. 48, no. 11, pp. 2049–2059, 1993, doi: 10.1016/0009-2509(93)80081-Z.

[16] A. Gordiychuk, M. Svanera, S. Benini, and P. Poesio, Size distribution and Sauter mean diameter of micro bubbles for a Venturi type bubble generator, *Experimental Thermal and Fluid Science*, vol. 70, pp. 51–60, 2016, doi: 10.1016/j.expthermflusci.2015.08.014.

[17] J. Huang *et al.*, A visualized study of bubble breakup in small rectangular Venturi channels, *Exp. Comput. Multiph. Flow*, vol. 1, no. 3, pp. 177–185, Sep. 2019, doi: 10.1007/s42757-019-0018-x.

[18] J. Huang *et al.*, An investigation on the performance of a micro-scale Venturi bubble generator, *Chemical Engineering Journal*, vol. 386, p. 120980, Apr. 2020, doi: 10.1016/j.cej.2019.02.068.

[19] C. H. Lee, H. Choi, D.-W. Jerng, D. E. Kim, S. Wongwises, and H. S. Ahn, Experimental investigation of microbubble generation in the venturi nozzle, *International Journal of Heat and Mass Transfer*, vol. 136, pp. 1127–1138, Jun. 2019, doi: 10.1016/j.ijheatmasstransfer.2019.03.040.

[20] L. Putri, W. Endra, and F. Martino, Performance of Porous-Venturi Microbubble Generator for Aeration Process, vol. 2, no. 2, pp. 73–80, 2017.

[21] A. Yadav, A. Kumar, and S. Sarkar, Performance evaluation of venturi aeration system, *Aquacultural Engineering*, vol. 93, p. 102156, May 2021, doi: 10.1016/j.aquaeng.2021.102156.

[22] A. Yadav and S. M. Roy, An artificial neural network-particle swarm optimization (ANN-PSO) approach to predict the aeration efficiency of venturi aeration system, *Smart Agricultural Technology*, vol. 4, p. 100230, Aug. 2023, doi: 10.1016/j.atech.2023.100230.

[23] L. Zhao, L. Sun, Z. Mo, J. Tang, L. Hu, and J. Bao, An investigation on bubble motion in liquid flowing through a rectangular Venturi channel, *Experimental Thermal and Fluid Science*, vol. 97, pp. 48–58, Oct. 2018, doi: 10.1016/j.expthermflusci.2018.04.009.

[24] L. Zhao *et al.*, Effects of the divergent angle on bubble transportation in a rectangular Venturi channel and its performance in producing fine bubbles, *International Journal of Multiphase Flow*, vol. 114, pp. 192–206, May 2019, doi: 10.1016/j.ijmultiphaseflow.2019.02.003.

[25] M. Sadatomi, A. Kawahara, K. Kano, and A. Ohtomo, Performance of a new micro-bubble generator with a spherical body in a flowing water tube, *Experimental Thermal and Fluid Science*, vol. 29, no. 5, pp. 615–623, 2005, doi: 10.1016/j.expthermflusci.2004.08.006.

[26] D. I. Mawarni *et al.*, Statistical Characterization of Bubble Breakup Flow Structures in Swirl-Type Bubble Generator Systems, *ASEAN J. Chem. Eng.*, vol. 23, no. 1, p. 62, Apr. 2023, doi: 10.22146/ajche.78558.

[27] X. Wang *et al.*, Performance comparison of swirl-venturi bubble generator and conventional venturi bubble generator, *Chemical Engineering and Processing - Process Intensification*, vol. 154, p. 108022, Aug. 2020, doi: 10.1016/j.cep.2020.108022.

[28] X. Wang *et al.*, Bubble breakup in a swirl-venturi microbubble generator, *Chemical Engineering Journal*, vol. 403, p. 126397, Jan. 2021, doi: 10.1016/j.cej.2020.126397.

[29] X. Xu, X. Ge, Y. Qian, B. Zhang, H. Wang, and Q. Yang, Effect of nozzle diameter on bubble generation with gas self-suction through swirling flow, *Chemical Engineering Research and Design*, vol. 138, pp. 13–20, Oct. 2018, doi: 10.1016/j.cherd.2018.04.027.

[30] A. Basso, F. A. Hamad, and P. Ganesan, Effects of the geometrical configuration of air–water mixer on the size and distribution of microbubbles in aeration systems, *Asia-Pacific Journal of Chemical Engineering*, vol. 13, no. 6, pp. 1–11, 2018, doi: 10.1002/apj.2259.

[31] K. Terasaka, A. Hirabayashi, T. Nishino, S. Fujioka, and D. Kobayashi, Development of microbubble aerator for waste water treatment using aerobic activated sludge, *Chemical Engineering Science*, vol. 66, no. 14, pp. 3172–3179, 2011, doi: 10.1016/j.ces.2011.02.043.

[32] J. Huang *et al.*, A review on bubble generation and transportation in Venturi-type bubble generators, *Experimental and Computational Multiphase Flow*, vol. 2, no. 3, pp. 123–134, 2020, doi: 10.1007/s42757-019-0049-3.

[33] A. Yoshida, O. Takahashi, Y. Ishii, Y. Sekimoto, and Y. Kurata, Water purification using the adsorption characteristics of microbubbles, *Japanese Journal of Applied Physics, Part 1: Regular Papers and Short Notes and Review Papers*, vol. 47, no. 8 PART 1, pp. 6574–6577, 2008, doi: 10.1143/JJAP.47.6574.

[34] S. Uesawa, A. Kaneko, and Y. Abe, Measurement of void fraction in dispersed bubbly flow containing micro-bubbles with constant electric current method, 2012, doi: 10.1016/j.flowmeasinst.2012.03.010.

[35] D. Deendarlianto, I. Indarto, W. E. Juwana, L. P. Afisna, and F. M. Nugroho, Performance of Porous-Venturi Microbubble Generator for Aeration Process, *JEMMME*, vol. 2, no. 2, Dec. 2017, doi: 10.22219/jemmme.v2i2.5054.

[36] L. Sun *et al.*, Characteristics and mechanism of bubble breakup in a bubble generator developed for a small TMSR, *Annals of Nuclear Energy*, vol. 109, pp. 69–81, Nov. 2017, doi: 10.1016/j.anucene.2017.05.015.

[37] L. Zhao *et al.*, A visualized study of the motion of individual bubbles in a venturi-type bubble generator, *Progress in Nuclear Energy*, vol. 97, pp. 74–89, May 2017, doi: 10.1016/j.pnucene.2017.01.004.

[38] G. Ding, Z. Li, J. Chen, and X. Cai, An investigation on the bubble transportation of a two-stage series venturi bubble generator, *Chemical Engineering Research and Design*, vol. 174, pp. 345–356, Oct. 2021, doi: 10.1016/j.cherd.2021.08.022.

[39] J. Huang, L. Sun, M. Du, Z. Mo, and L. Zhao, A visualized study of interfacial behavior of air–water two-phase flow in a rectangular Venturi channel, *Theoretical and Applied Mechanics Letters*, vol. 8, no. 5, pp. 334–344, 2018, doi: 10.1016/j.taml.2018.05.004.

[40] F. Reichmann, M.-J. Koch, and N. Kockmann, Investigation of Bubble Breakup in Laminar, Transient, and Turbulent Regime Behind Micronozzles, in *ASME 2017 15th International Conference on Nanochannels, Microchannels, and Minichannels*, Cambridge, Massachusetts, USA, Aug. 2017, p. V001T03A001. doi: 10.1115/ICNMM2017-5540.

[41] J. Li, Y. Song, J. Yin, and D. Wang, Investigation on the effect of geometrical parameters on the performance of a venturi type bubble generator, *Nuclear Engineering and Design*, vol. 325, pp. 90–96, Dec. 2017, doi: 10.1016/j.nucengdes.2017.10.006.

[42] S. Mardikus, Effects of Shock Wave Phenomenon on Different Convergent Lengths in the Mixing Chamber of the Steam Ejector, *International Journal of Applied Sciences and Smart Technologies*, vol. 3, no. 1, pp. 93–100, Jun. 2021, doi: https://dx.doi.org/10.24071/ijasst.v3i1.3249.

[43] D. I. Mawarni, W. E. Juwana, K. A. Yuana, W. Budhijanto, Deendarlianto, and Indarto, Hydrodynamic characteristics of the microbubble dissolution in liquid using the swirl flow type of microbubble generator, *Journal of Water Process Engineering*, vol. 48, p. 102846, Aug. 2022, doi: 10.1016/j.jwpe.2022.102846.

[44] P. Cramers, A. Beenackers, and van L. Dierendonck, Hydrodinamics and mass transfer characteristics of a loop-venturi reaktor with a downflow liquid jet ejector, *Chemical Engineering Science*, vol. 47, no. 13/14, pp. 3557–3564, 1992.

[45] I. Catrawedarma, D. Deendarlianto, and I. Indarto, Statistical Characterization of Flow Structure of Air–water Two-phase Flow in Airlift Pump–Bubble Generator System, *International Journal of Multiphase Flow*, vol. 138, no. 103596, 2021.

[46] D. H. Sharp, An overview of Rayleigh-Taylor instability, *Physica D: Nonlinear Phenomena*, vol. 12, no. 1–3, pp. 3–18, Jul. 1984, doi: 10.1016/0167-2789(84)90510-4.

[47] E. N. Sari, A. Fiveriati, N. Rusti, J. Rulianto, R. Bhiqman Susanto, and I. Catrawedarma, Visual and Pressure Signal Investigations on Bubble Produced by Ejector Bubble Generator, *E3S Web Conf.*, vol. 483, p. 03020, 2024, doi: 10.1051/e3sconf/202448303020.

This page intentionally left